ORIENTAL JOURNAL OF CHEMISTRY
An International Open Access, Peer Reviewed Research Journal
www.orientjchem.org
ISSN: 0970-020 X
CODEN: OJCHEG
2025, Vol. 41, No.(5):
Pg. 1653-1658

Surfactant-Assisted Synthesis of Polyindole/MWCNT Nanocomposites: Physicochemical Characterization and DC Electrical Conductivity Studies

NAIF AHMED ALSHEHRI

Department of Physics, College of Science, Al-Baha University, Al-Baha, Saudi Arabia.
*Corresponding author E-mail: nalshehri@bu.edu.sa

http://dx.doi.org/10.13005/ojc/410519

(Received: July 12, 2025; Accepted: September 01, 2025)

ABSTRACT

A nanocomposite material comprising polyindole (PI), cetyltrimethylammonium bromide (CTAB), and multi-walled carbon nanotubes (MWCNTs) was synthesized to investigate its DC electrical conductivity and physicochemical characteristics. The synthesis was carried out through in-situ chemical oxidative polymerization, where CTAB acted as a surfactant to aid uniform dispersion. The DC electrical conductivity was measured using the standard four-point probe technique typically employed for semiconductor materials. Additionally, the effect of temperature on electrical conductivity retention and thermal stability was assessed. Comprehensive characterization was performed using Fourier transform infrared spectroscopy (FTIR), thermogravimetric analysis (TGA), X-ray diffraction (XRD), scanning electron microscopy (SEM), and transmission electron microscopy (TEM) to evaluate the material's structural and morphological features. At 30°C, the PI/CTAB/MWCNT nanocomposite exhibited a DC electrical conductivity of 6.3×10^{-5} cm^{-1}. The prepared PI composite is stable at high temperatures and offers potential applications in energy devices like batteries, fuel cells, and supercapacitors.

Keywords: Conducting polymers, Four-probe electrical conductivity measurement, Multi-walled carbon nanotubes, Polyindole, Surfactant-assisted polymerization.

INTRODUCTION

With the development in technology and awareness of global warming, the industrial interest has shifted towards advanced materials with desirable properties in terms of low cost, stability, and easy fabrication[1,2]. For this purpose, instead of using expensive metal conductors, pose the threat of corrosion and metal poisoning, semiconductors like conducting polymers have emerged as promising alternatives[3]. Conducting polymers have played a major role in revolutionizing material science by offering unmatched properties[4]. Conducting polymers have excellent conductivity due to the delocalization of π electrons[5,6]. The long-chain structure of conducting polymers imparts greater stability and flexibility to the compound. Among many conducting polymers, polyindole[7] stands out due to its exceptional chemical stability, tunable electrical properties, and easy synthesis[8] making it suitable for application in energy storage, supercapacitors, and sensing devices[9,10].

DC electrical conductivity is an inherent property and is influenced by factors such as the alignment of the polymeric chain, doping, charge carrier routes and polymeric concentration in the matrix[11-13]. In the study conducted by Asif *et al.,* the electrical conductivity of the polypyrrole/ polyantimonic acid composite was found to increase from 3.94×10^{-9} to 2.37×10^{-4}S cm^{-1} by increasing the pyrrolic concentration from 23.33 to 40%, respectively[14]. For semiconductors, electrical conductivity increases with an increase in temperature[15] and decreases at very high temperatures. The stability of the compound defines the retention of the DC electrical conductivity for longer periods. Therefore, the fabrication of a nanocomposite that enhances the stability of the polyindole was done by adding surfactant and carbon nanotubes[16,17]. The surface area of the nanocomposite was greatly increased by adding cetyltrimethylammonium bromide (CTAB) surfactant, which improves the alignment of the polymeric chain[18]. This improves the bulk properties of the composite and makes the composite more perceivable by the instrument. Numerous research studies have been done using MWCNT, which is known to have excellent conductivity[19]. Incorporating carbon nanotube filler in the conducting polymer matrix imparts exceptional thermal stability, strength, and conductivity to the composite material. CTAB enhances the dispersion of MWCNT and improves the polymerization process. DC electrical conductivity of polyaniline (PANI) was investigated by Shahid *et al.,*[20]. The research reveals that the PANI nanocomposite follows an Arrhenius-type temperature dependence. Another study on polypyrrole/CTAB/vitamin K3/glucose oxidase composite was performed by Maha *et al.,*[21] which clearly explained the increasing electrical behavior of the semiconductors with increasing temperature up to an optimum value of 2.1×10^{-2}S cm^{-1}, after which a slight decrease in the conductivity was observed, due to the loss of dopants and their reactions with the material. This work aims to analyze the synergistic properties of CTAB-assisted polyindole and MWCNT nanocomposite, resulting in an enhanced electrical conductivity behavior determined using the four-probe technique. The physicochemical properties of the resulting nanocomposite are studied using FTIR, TGA, XRD, SEM and TEM techniques. The as-synthesized PI/CTAB/MWCNT composite displays thermal stability and superior electrical properties proving its potential in a wide range of applications including sensors, microelectronics, batteries[22], fuel cells[23], supercapacitors and energy storage devices[24].

MATERIALS AND METHODS

Indole (99% purity), cetyltrimethylammonium bromide (CTAB), chloroform ($CHCl_3$), and ferric chloride ($FeCl_3$) were sourced from Central Drug House Pvt. Ltd., India, while multi-walled carbon nanotubes (MWCNTs) were purchased from Sigma-Aldrich. All experimental procedures were carried out using double-distilled water. The DC electrical conductivity of the polyindole/MWCNT composite was measured using a four-point probe conductivity meter (SES Instruments, Roorkee, India). Morphological analysis was conducted via scanning electron microscopy (SEM, Carl Zeiss Supra 55) and transmission electron microscopy (TEM, TECHNAI T20, 200 keV, FEI), with TEM samples mounted on carbon-coated copper grids. Thermal stability was examined using thermogravimetric analysis (TGA, Perkin Elmer), and crystallographic studies were performed using X-ray diffraction (XRD, Panalytical X'Pert Pro). Fourier transform infrared spectroscopy was performed using Cary 630, Agilent Technology, in the range of 400 to 4000 cm^{-1}.

Preparation of polyindole composite

Polyindole was synthesized by *in-situ* polymerization of the indole monomer through chemical oxidation over the surface of the surfactant cetyltrimethylammonium bromide (CTAB), wherein Ferric chloride ($FeCl_3$) was used as the oxidizing agent. 2.25 g of indole monomer was dissolved in 50 mL of chloroform on a magnetic stirrer. 100 mg of CTAB and an aqueous suspension of 10 mg of pristine MWCNTS were added to the monomeric solution. After thorough optimization, monomer-to-oxidant concentration was kept at a ratio of 1:4 and the indole solution was then poured into the aqueous solution of ferric chloride. The mixture was left for overnight stirring to complete the process of polymerization. A dark greenish-black polymerized precipitate was obtained which was filtered out using Whatman filter paper no. 1 and washed with distilled water till the filtrate appeared colorless. The precipitate was dried in a hot air oven at 40°C for 6 hours[25].

RESULTS AND DISCUSSION

TGA

The thermal stability of the PI/CTAB/MWCNT composite was evaluated through thermogravimetric analysis (TGA). An initial weight loss of approximately 8% up to 100°C is attributed to the evaporation of physically adsorbed water. This is followed by an additional weight reduction of about 5.68% in the temperature range of 100–270°C, likely due to the release of interstitial water molecules[26]. At around 400°C, continuous weight loss is observed due to PI backbone decomposition along with the complete oxidation of MWCNTs[27]. Above this, decomposition terminates and a smooth horizontal section is observed at around 600°C indicating the formation of a carbon-black mass[28,29].

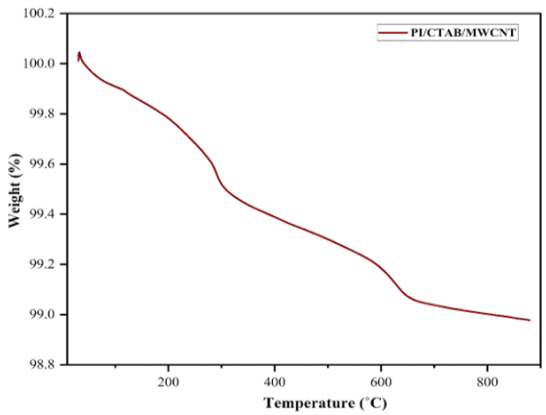

Fig. 1. TGA graph of PI/CTAB/MWCNTs nanocomposite

FTIR

Figure 2 presents the FTIR spectra of PI, PI/CTAB, and PI/CTAB/MWCNT. The absorption bands observed at approximately 1564 cm^{-1} and 1624 cm^{-1} correspond to C–C stretching vibrations within the benzenoid ring of the indole structure, whereas the peak near 1098 cm^{-1} is characteristic of C=N stretching vibrations[30]. Additionally, the signals at around 1451 cm^{-1} and 1550 cm^{-1} are attributed to C–N stretching modes, and the band near 735 cm^{-1} is associated with out-of-plane bending vibrations of the benzene ring[31]. Significant differences are observed between the PI/CTAB and PI/CTAB/MWCNT spectra, and after MWCNT was added to the composite, the bands seem to have significantly intensified. The presence of all the assigned peaks in the PI/CTAB/MWCNT spectrum indicates the successful association of the different components in this composite[32,33].

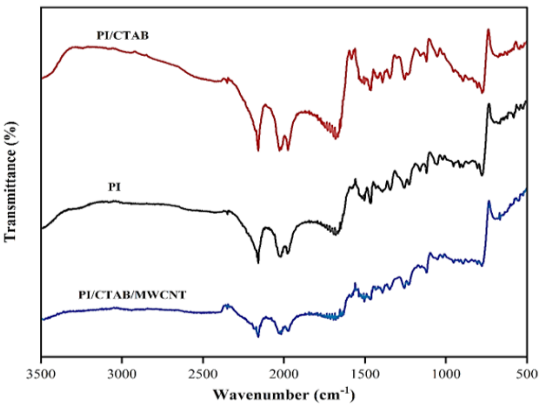

Fig. 2. FTIR spectra of PI, PI/CTAB and PI/CTAB/MWCNTs

X-ray diffraction

X-ray diffraction analysis was carried out to examine the crystalline structure of the synthesized composite. As shown in Fig. 3(a), a distinct and intense peak is observed at 2θ = 26.7°. This peak is ttributed to the semi-crystalline nature of polyindole. With the addition of surfactant significant increase in the crystallinity is observed as shown in Fig. 3(b). As per the literature reported, the XRD peaks of MWCNT fall in the same region or vicinity as that of polyindole. However, slight differences may occur after the formation of the composite. The remaining peaks can be attributed to the surfactant CTAB. Whereas in the absence of MWCNT as represented in Fig. 3(b), only CTAB gives more sharp peaks along with polyindole. But in the composite of MWCNT, some shift in the peaks is seen. Significant peaks of MWCNT at 24.6, 33.9, and 42.99 (2 theta) values indicate successful incorporation of MWCNT with a distinct peak of polyindole at 26.7 (2 theta) value as shown in Fig. 3(c). The mean crystal size of the PI/CTAB/MWCNTs nanocomposite was also calculated using Debye-Scherrer's equation[34] and was found to be 18.4 nm.

$$D = K\lambda/\beta\cos\theta$$

SEM and TEM analyses

The morphological behavior of the composite was studied through SEM and TEM images of the composite. As evident from the image, Fig. 4(a), polyindole has a rough morphology and slightly globular structure. However, Fig. 4(b) shows that with the addition of the surfactant, the surface morphology has become smooth. Fig. 4(c) shows the change in morphology with the edition of MWCNTs.

In Fig. 4(d) the PI/CTAB/MWCNT composite filamentous and small globular-like structure is visible, confirming the incorporation of MWCNT with polyindole supported over the surfactant.

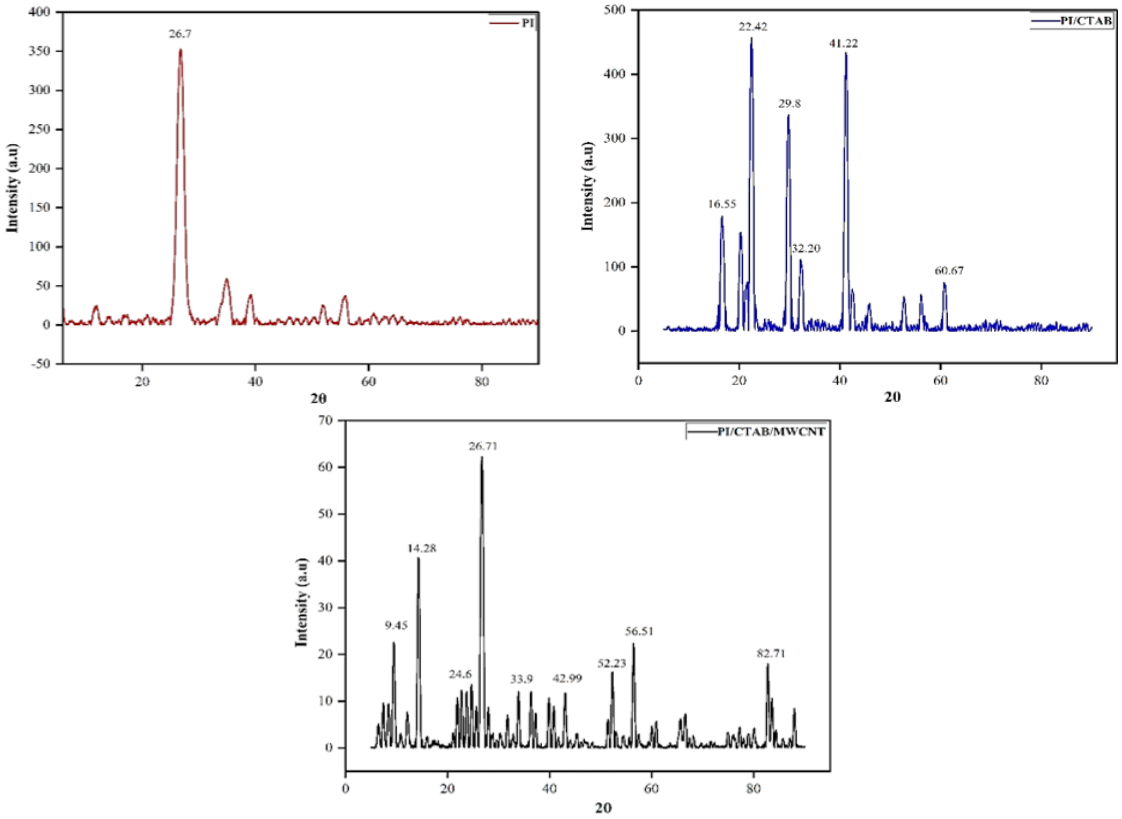

Fig. 3. XRD of (a) PI, (b) PI/CTAB, (c) PI/CTAB/MWCNTs

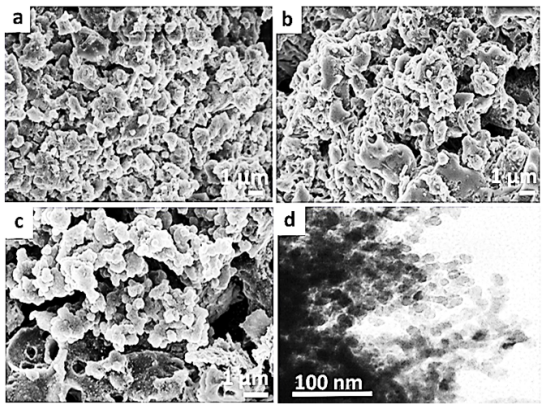

Fig. 4. SEM micrographs of (a) polyindole, (b) polyindole with CTAB, (c) polyindole/CTAB/MWCNT composite, and (d) TEM micrograph of the PI/CTAB/MWCNT nanocomposite

Electrical conductivity evaluation

For energy-related applications such as batteries, supercapacitors, and fuel cells, thermal stability is a critical parameter in assessing the suitability of a composite material. The DC electrical conductivity of the polyindole-based composite was evaluated using a four-point probe conductivity measurement setup. Prior to measurement, the composite was thoroughly dried and then compressed into pellets under hydraulic pressure to eliminate any interference from protonic conduction in the electrical response of the material[35]. The electrical conductivity (σ) was determined using the following equations:

$$\sigma = \sigma_o/G_7\ (W/S) \quad (1)$$

Here, σ denotes the electrical conductivity expressed in S cm^{-1}, while G_7 (W/S) is the correction factor accounting for a non-conductive bottom surface. In this expression, W refers to the width of the sample (in cm) and S represents the distance between adjacent probes (in cm). The value of the correction factor depends on the ratio of W to S.

$$G_7 \times (W/S) = 2S\ (\ln 2)/W \quad (2)$$

and

$$\sigma_o\sigma = I / V \times (2\pi S) \quad (3)$$

Where V and I are the voltage (V) and current (A) respectively.

The prepared PI/CTAB/MWCNT composite was subjected to elevated temperatures to understand its conductivity (σ) pattern variation. The electrical conductivity of the composite was tested at 50, 70, 90, 110, 130, and 150°C for 80 sec at each temperature, separated by a time gap of 15 minute. As the graph shows in Fig. 5, the composite exhibits stable electrical conductivity at lower temperatures, followed by a slight increase in conductivity at around 70–90°C, which can be attributed to the semiconducting characteristics of polyindole[36].

Table 1: DC conductivity of polyindole composite at room temperature

Sample	Conductivity (S cm^{-1})	Resistivity (Ωcm)
PI	5.2×10^{-6}	19.23×10^{4}
PI/CTAB	9.4×10^{-6}	10.64×10^{4}
PI/CTAB/MWCNT	6.3×10^{-5}	15.87×10^{3}

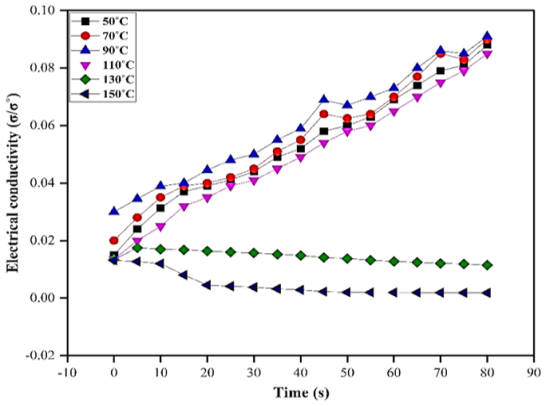

Fig. 5. Isothermal stability of PI/CTAB/MWCNTs nanocomposite regarding DC electrical conductivity retention at different temperatures

To evaluate the stability of the composite in terms of electrical conductivity retention, it was subjected to five consecutive heating cycles, each reaching a maximum temperature of 200°C. DC electrical conductivity was measured after each cycle using the four-point probe method, with a 60 minute interval between successive cycles. For each cycle, conductivity values were plotted as log σ against 1000 T^{-1} (K). As illustrated in Fig. 6, the conductivity behavior across the heating and cooling cycles followed the Arrhenius relationship, showing only a marginal decline in the last two cycles[37].

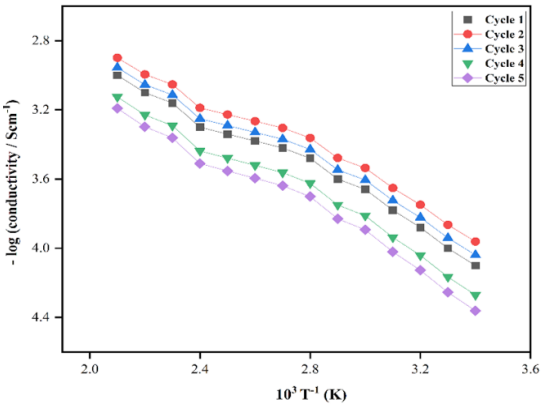

Fig. 6. Arrhenius plot of the PI/CTAB/MWCNT composite illustrating the preservation of DC electrical conductivity across multiple heating–cooling cycles

The five cycles show only minor differences in conductivities over a wide temperature range of 30–200°C, proving that the fabricated PI/CTAB/MWCNT composite is stable even under severe oxidizing temperatures due to the synergistic interactions of surfactant-assisted polyindole with MWCNTs. The percentage retention of electrical conductivity of the polyindole/MWCNT nanocomposite under different exposure environments was studied. The results presented in Fig. 7 indicate that the composite remains stable in terms of electrical conductivity retention for up to 20 days. Upon exposure to the laboratory environment for about 90 days, the composite retained approximately 60% of its electrical conductivity. These findings demonstrate that the polyindole/MWCNT nanocomposite exhibits good environmental stability with respect to electrical conductivity retention.

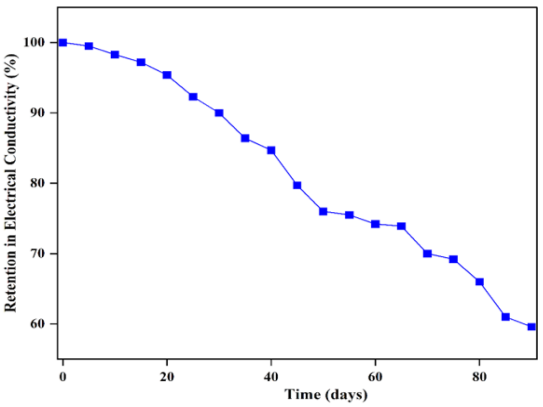

Fig. 7. Percentage retention of electrical conductivity as a function of exposure time in the environment

CONCLUSION

The prepared PI/CTAB/MWCNTs

nanocomposite shows modest electrical output and excellent thermal stability. In the resulting composite, Polyindole acts as a versatile conducting polymer offering tunable properties with optimum current retention capacity. The DC electrical conductivity of the final PI/CTAB/MWCNTs was found to be 6.3×10^{-5} S cm^{-1} at room temperature. The synergistic effects of the various components in the composite provide unmatched stability even at high temperatures, making PI/CTAB/MWCNTs an excellent candidate for applications in energy devices like batteries, fuel cells, sensors and supercapacitors.

ACKNOWLEDGMENT

The author thanks Al-Baha University Faculty of Science, Al Baha, Saudi Arabia for providing research facilities.

Conflict of Interest

The author(s) do not have any conflict of interest.

REFERENCES

1. Davis, F.; Higson, S. P. J., *Biosens. Bioelectron.*, **2007**, *22*, 1224–1235.
2. Heller, A., *Anal. Bioanal. Chem.*, **2006**, *385*, 469–473.
3. Khoo, K. S.; Chia, W. Y.; Ying, D.; Tang, Y.; Energies. 2020, 13, 892.
4. Ramanavicius, S.; Ramanavicius, A., *Polymers.*, **2021**, *13*, 49.
5. Awuzie, C. I., *Mater. Today Proc.*, **2017**, *4*, 5721-5726.
6. Sintayehu, Y. D.; Murthy, H. C. A., *Adv. Mater. Lett.*, **2019**, *10*, 524–532.
7. Ding, H.; Hussein, A. M.; Ahmad, I.; Latef, R.; Abbas, J. K.; Ali, A. T. A.; Saeed S. M.; Elawady, A., *Alexandria Engg. J.*, **2024**, *88*, 253-267.
8. Nezakati, T.; Seifalian, A.; Tan, A.; Seifalian, A. M.; *Chem. Rev.*, **2018**, 118, 6766-6843.
9. Rout, C. S., *RSC Adv.,* **2021**, *11*, 5659-5697.
10. Barde, R. V.; Nemade, K. R.; Waghuley, S. A., *Chem. Phys. Impact.*, **2022**, *5*, 100100.
11. Mehtab, S.; Zaidi, M. G. H.; Singha, K.; Arya, B.; Siddiqui, T. I., *Mat. Sci. Res. India.*, **2019**, *16*, 97-102.
12. Le, T. H.; Kim, Y.; Yoon, H., *Polymers.*, **2017**, *9*, 150.
13. Kausar, A., *J. Macromol. Sci. Part A.*, **2017**, *54*, 640-653.
14. Khan, A. A.; Alam, M. M.; Inamuddin.; Mohammad, F., *J. Electroanal. Chem.*, **2004**, *572*, 67-78.
15. Haque, S. U.; Nasar, A.; Inamuddin.; Rahman, M. M., *Sci. Rep.*, **2020**, *10*, 10428.
16. Trujillo, D. J.; Maldonado, L. V.; Barragán, J. J., *Sci. Rep.*, **2023**, *13*, 4810.
17. Montoya, O. D.; Serra, F. M.; De Angelo, C. H., *Electronics.*, **2020**, *9*, 1352.
18. Perveen, R.; Nasar, A.; Inamuddin., Asiri, A. M.; Mishra, A. K., *Int. J. Hydr. Energy.*, **2018**, *43*, 15144-15154.
19. Phromviyo, N.; Boonlakhorn, J.; Posi, P.; Thongbai, P.; Chindaprasirt, P., *Polymers.*, **2022**, *14*, 320.
20. Ansari, S.P.; Mohammad, F., *Polym. Compos.* **2016**, *24*, 273-280.
21. Male, U.; Shin, B. K.; Huh, D. S., *Macromol. Res.*, **2017**, *25*, 1121–1128.
22. Shaban, S. M.; Kang, J.; Kim, D. H., *Compos. Commun.*, **2020**, *22*, 100537.
23. Marriam, I.; Wang, Y.; Tebyetekerwa, M., *Chem. Commun.*, **2020**, *33*, 336-359.
24. Mudila, H.; Prasher, P.; Kumar, M.; Kumar, A.; Zaidi, M. G. H.; Kumar, A., *Mater. Renew. Sustain. Energy.*, **2019**, *8*, 9.
25. Perveen, R.; Inamuddin.; Haque, S. U., *Sci. Rep.*, **2017**, *7*, 13353.
26. Montanheiro, T. L.; Durán, N.; Lemes, A. P., *J. Mater. Res.*, **2015**, *30*, 55–65.
27. Chamorro, A. F.; Lerma, T. A.; Palencia, M., *Water.*, **2024**, *16*, 1860.
28. Shettigar, R. R.; Misra, N. M.; Patel, K., *J. Petrol. Explor. Prod. Technol.*, **2018**, *8*, 597–606.
29. Yuan, S.; Zheng, Y.; Chua, C. K.; Yan, Q.; Zhou, K., *Compos. Part A. Appl. Sci. Manuf.,* **2018**, *105*, 203-213.
30. Inamuddin.; Shakeel, N.; Ahamed, M. I., *Sci. Rep.*, **2020**, *10*, 5052.
31. Khan, M.; Inamuddin., *Sci. Rep.*, **2024**, *14*, 3324.
32. Humayun, H.; Begum, B.; Bilal, S.; Shah, A. H.; Röse, P., *Nanomaterials.*, **2023**, *13*, 618.
33. Chhattise, P.; Handore, K.; Horne, A.; Mohite, K.; Chaskar, A.; Dallavalle, S.; Chabukswar, V., *J. Chem. Sci.*, **2016**, *128*, 467-475.
34. Chulliyote, R.; Hareendrakrishnakumar, H.; Raja, M.; Gladis, J. M.; Stephan, A. M., *Sust. Energy Fuels.*, **2017**, *1*, 1774-17811.
35. Mondal, S.; Sen, S.; Kumar, A.; Mudila, H.; *Results Opt.*, **2023**, *13*, 100556.
36. Onthong, S.; Pongprayoon, T.; Rear, E. A., *ACS Appl. Polym. Mater.*, **2025**, *7*, 187–199.
37. Chelly, A.; Glass, S.; Belhassen, J.; Karsenty, A., *Results Phys.*, **2023**, *48*, 106445.